# Multimicroprocessor-Based Robust Control of an AC Induction Servo Motor

YING-YU TZOU, MEMBER, IEEE, AND HSIANG-JUI WU

*Abstract*—**A multiloop feedback control system supplemented by a complementary controller is used to improve the drive performance of an ac induction servo motor and reduce sensitivity to parameter variations, nonlinear effects, and load disturbances. Based on the principle of field-oriented vector control, a software-based current-decoupled controller has been proposed. A simplified model of the current-decoupled induction motor has been used for the design and simulation of the proposed robust controller. Experimental results based on multimicroprocessor implementation are presented to illustrate improved response and reduced sensitivity.**

## I. Introduction

THE AC induction motor with its inherent low stator and rotor leakage reactance and lower rotor inertia can achieve significantly faster transient torque response and rotation at higher speed than the dc motor. Advances in microelectronics and variable-frequency static inverters now has made it possible to devise very sophisticated digital ac-servo drives of synchronous or asynchronous motors by using modern control system design methodology [1], [2]. Inverter-fed ac motors controlled by field-oriented vector control strategy implemented by state-of-the-art digital control methods are replacing dc motors in many applications where fast response is required, such as feed drives and spindle drives for high-performance machine tools.

Because of the fast development in automation technology, the demand for high-performance electrical servos has been increasing. To meet these high-performance servo requirements, it has become necessary to develop a controller that overcomes 1) the influence of nonlinear friction, 2) the influence of varying the motor's parameters, and 3) the influence of changing loads (such as inertia and viscous friction, etc.).

One of the servo mechanism systems, which guarantees asymptotic tracking and regulation independent of disturbances and arbitrary perturbations in the plant parameters, is called the robust controller by Davison [3]. However, as the robust controller has only an assurance of no steady-state error for assumed reference signals and disturbances, the improvement of transient responses in the presence of parameter variations is left, without any guide lines, to the controller designer.

Robust controllers that guarantee both the transient and steady-state responses of dc servo mechanism systems within specified bounds under large plant uncertainty due to parameter and load variations have become an important issue in recent years [4], [5]. A complementary controller based on the concept of two degrees of freedom [6] and a robust position controller based on the internal model principle [7] have been proposed by Ohishi *et al.* [8]. A feedforward integral–proportional (IP) controller with specified dominant pole has also been proposed by Bai and Tagawa [9]. These methods work satisfactorily for dc servo motor control but are scarcely used for high-performance ac induction servo motor control. One reason may be the model complexity of the induction machine, the other may be some unknown factors in digital controller realization and lack of experiences.

This paper presents the design and implementation of a multimicroprocessor-based digital ac induction servo drive by adopting the field-oriented vector control scheme for the torque-loop control and model reference complementary control schemes for velocity- and position-loop control.

A simplified model of the current-decoupled induction motor has been used for the design and simulation of the proposed robust controller. Simulation and experimental results have shown the effectiveness of the simplified model. Experimental results have also shown that the digital-type complementary controller based on two-degree-of-freedom theory with a multiloop robust position controller can effectively reduce the system sensitivity for both the parameter variations and the load torque disturbances.

## II. Decoupling Control and Modeling

The dynamic properties of an induction motor as a controlled plant can be described by a set of nonlinear differential equations linking the stator and rotor currents and voltages with the mechanical quantities torque, speed, and angular position. The analysis and control of such a plant becomes complicated because of intricate coupling between all the control inputs. This problem can be overcome by the control of field-oriented quantities which reduces the control of an ac induction motor to that of a separately excited dc motor [10]. In developing the field-oriented vector control techniques, the rotor flux may be characterized by an equivalent stator-based mag-

Paper IPCSD 89-25, approved by the Industrial Drives Committee of the IEEE Industry Applications Society for presentation at the 1988 Industry Applications Society Annual Meeting, Pittsburgh, PA, October 2–7. Manuscript released for publication July 25, 1989.

Y. Y. Tzou is with the Institute of Control Engineering, National Chiao-Tung University, 75 Po-Ai Street, Hsin Chus 30039, Taiwan, Republic of China.

H. J. Wu is with the Institute of Electronics, National Chiao-Tung University, 75 Po-Ai Street, Hsin Chu 30039, Taiwan, Republic of China.

IEEE Log Number 9034288.

0093-9994/90/0500-0441$01.00 

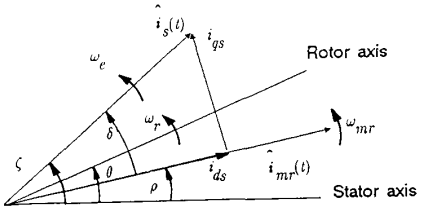


Fig. 1. Principle of field-oriented vector control.

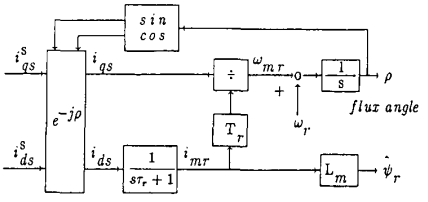


Fig. 2. Rotor flux model in synchronous rotating reference frame.

netizing current containing a component for magnetic leakage (Fig. 1)

$$\hat{i}_{mr} = \hat{i}_s + (1+\sigma_r)\hat{i}_r e^{j\theta} = i_{mr} e^{j\rho} \tag{1}$$

where $\sigma_r = (L_r - L_m)/L_m$ is the rotor leakage factor. All symbols are listed in the Nomenclature at the end of the paper. The rotor flux vector $\hat{\psi}$ can be expressed as

$$\hat{\psi} = L_m \hat{i}_{mr} e^{-j\theta}. \tag{2}$$

Based on the $d$–$q$ two-axis theory and field-oriented vector control principle, when fixing the $d$ axis on the synchronously rotating rotor flux vector $\hat{\psi}$, the torque generation of a symmetrical induction motor under decoupling control can be derived as [11]

$$i_{ds} = \frac{\tau_r}{L_r}\frac{di_{mr}}{dt} + \frac{1}{L_m} i_{mr} \tag{3}$$

$$i_{qs} = (\omega_e - \omega_r)\tau_r i_{mr} = \omega_{mr}\tau_r i_{mr} \tag{4}$$

$$T_e = \frac{3}{2}\frac{P}{2}\frac{L_m}{1+\sigma_r} i_{mr} i_{qs}. \tag{5}$$

Its mechanical dynamics with the lumped inertia $J_m$ and the net load torque $T_l$ can be expressed as

$$J_m \frac{d\omega_m}{dt} = T_e - T_l(\theta, \omega_m, t) \tag{6}$$

$$\frac{d\theta}{dt} = \omega_m. \tag{7}$$

Having up-to-date information of the rotor flux vector is essential for decoupling control since this is the basis of coordinate transformation. A flux model based on the field coordinate as shown in Fig. 2 has been used for the computation of the rotor flux. This flux model in field coordinates is preferable because of its simplicity and potential accuracy, because the output signals are constant in steady state, and because the flux sensing can operate down to zero frequency since no open-ended integration is needed which would be subject to drift.

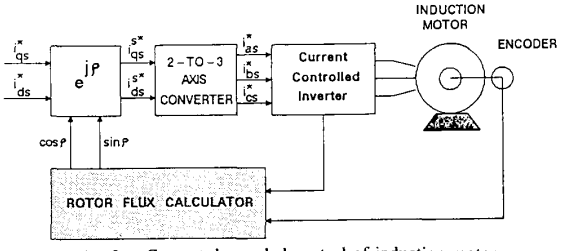


Fig. 3. Current-decoupled control of induction motor.

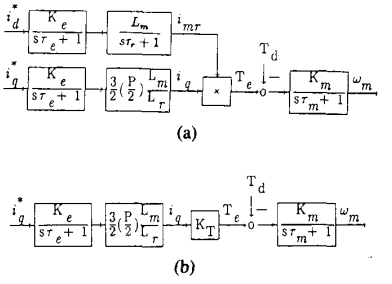


Fig. 4. (a) Block diagram of induction motor model under current-decoupled control. (b) Simplified model in constant-torque operation range.

The mathematical model of a current-decoupled ac induction motor (Fig. 3) is shown in Fig. 4(a). When the motor is operating in its constant-torque region (with fixed field exciting current) this model can be reduced to a second-order system as shown in Fig. 4(b). Note that the current-controlled PWM inverter has also been included in this simplified equivalent model. Therefore, its input is the desired torque current command. This simplified model has been used to illustrate the design procedure of the proposed robust servo controller which can be further applied to the complete model when operating over the full speed control range.

The transfer function of this current-decoupled ac servo motor can be written as

$$P(s) = \frac{\omega_m(s)}{i_q(s)} = K_T \frac{K_e}{s\tau_e + 1}\frac{K_m}{s\tau_m + 1} \tag{8}$$

$$K_T = \frac{3}{2}\frac{P}{2}\frac{L_m}{1+\sigma_r} i_{mr} \tag{9}$$

$$\theta_m(s) = \frac{1}{s}\omega_m(s) \tag{10}$$

where $\theta_m$ and $\omega_m$ are the load-shaft angular position and velocity, respectively, $i_q$ is the torque current command sent to the current-decoupled vector controller, $i_{mr}$ is the magnetizing current, $\tau_e$ and $K_e$ are the corresponding electrical time constant and gain of the current loop controller, and $\tau_m$ and $K_m$ are the equivalent mechanical time constant and gain of the connected load. Note that $\tau_m$ and $K_m$ of the simplified model are defined to model the mechanical dynamics of the motor and its connected load. These parameters can be obtained either by measurements or some system identification techniques. MKS units are used throughout this paper.

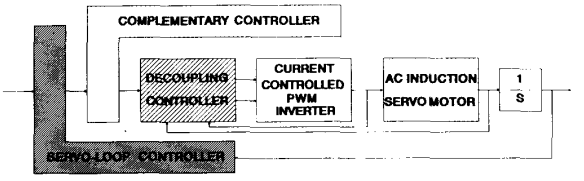


Fig. 5. Simplified structure of robust ac induction servo system.

## III. Robust Control Strategy

The simplified structure of the proposed robust control scheme of an ac induction servo motor is shown in Fig. 5. This digital robust ac induction servo controller is composed of four major units: 1) the PWM controller, 2) the torque decoupling controller, 3) the model reference complementary controller, and 4) the servo-loop controller.

As a control system is usually designed on the basis of the mathematical model representing the nominal dynamics of the plant, the designed target may not be attained when plant dynamics vary significantly from nominal values. The model reference complementary controller determines the sensitivity to parameter and load variations, while the servo-loop controller determines the overall performance indices such as rise time, damping characteristics, stiffness, and steady-state error. This complementary controller acts as a conditional feedback controller because the nominal model is explicitly included in the control system. The merit of this design method is that any type of controller can be adopted as a servo-loop controller because there is no interference between the complementary controller and servo-loop controller [6], [8].

The detailed block diagram of the proposed multiloop robust position servo controller is shown in Fig. 6, where $P(s)$ represents the plant dynamics, $P_m(s)$ is the reference model representing the nominal plant dynamics, $H(s)$ is the plant deviation compensator chosen to be a gain times the inverse of the nominal dynamics, and $D(s)$ is the servo-loop controller. As $\beta$ is increased, the complemented plant dynamics will be reduced to the transfer function of the nominal plant dynamics; therefore, the system is more insensitive to parameter variations.

## IV. Design Procedure

The design procedure of the proposed multiloop robust controller can best be illustrated by the following example.

### *Step 1—Define the Nominal Plant $P_m(s)$*

According to the plant load and parameter variations range as shown in Table I, the designer can classify some extreme testing conditions as shown in Table II. Their corresponding frequency and time responses are shown in Fig. 7(a) and (b). For consideration of equal deviations from the normal operating condition when the system experiences parameter and load variations, the nominal plant is set at the normal operating (NO) condition.

### *Step 2—Determination of the Sampling Period $T_h$*

Digital implementation of the complementary controller may become unstable due to unsuitable selection of the sampling period $T_h$. In practical situation, maximum computation time of the complementary controller by the microprocessor was chosen as the sampling period. In the designed system, $T_h$ is set at 1 ms.

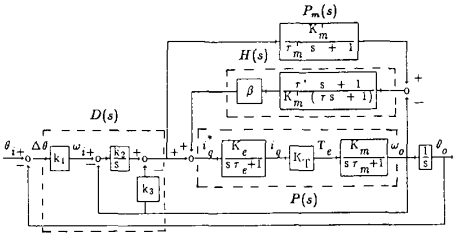


Fig. 6. Block diagram of proposed multiloop robust position servo controller.

TABLE I
MOTOR PARAMETER VARIATIONS

| | | |
|---|---|---|
| $K_e$ | 1.0 (A/A) | current gain |
| $\tau_e$ | 0.004 ~ 0.008 (s) | electrical time constant |
| $K_T$ | 0.5 ~ 1.0 (N·m/A) | torque constant |
| $K_m$ | 200 ~ 250 (rad/s)/Nm | motor gain |
| $\tau_m$ | 1.0 ~ 5.0 (s) | mechanical time constant |

TABLE II
TESTING CONDITION CLASSIFICATION UNDER PARAMETER VARIATION

| | | | | |
|---|---|---|---|---|
| N0 | $K_T = 0.8$ | $K_m = 250$ | $\tau_m = 1.6$ | $\tau_e = 0.004$ |
| N1 | $K_{T(\min)} = 0.5$ | $K_{m(\min)} = 200$ | $\tau_{m(\min)} = 1.0$ | $\tau_{e(\min)} = 0.004$ |
| N2 | $K_{T(\min)} = 0.5$ | $K_{m(\min)} = 200$ | $\tau_{m(\max)} = 5.0$ | $\tau_{e(\max)} = 0.008$ |
| N3 | $K_{T(\text{mid})} = 0.75$ | $K_{m(\text{mid})} = 225$ | $\tau_{m(\text{mid})} = 3.0$ | $\tau_{e(\text{mid})} = 0.006$ |
| N4 | $K_{T(\max)} = 1.0$ | $K_{m(\max)} = 250$ | $\tau_{m(\min)} = 1.0$ | $\tau_{e(\min)} = 0.004$ |
| N5 | $K_{T(\max)} = 1.0$ | $K_{m(\max)} = 250$ | $\tau_{m(\max)} = 5.0$ | $\tau_{e(\max)} = 0.008$ |

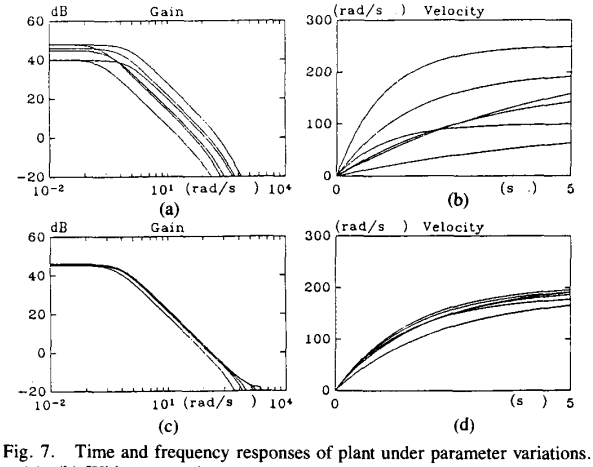


Fig. 7. Time and frequency responses of plant under parameter variations. (a), (b) Without complementary controller. (c), (d) With complementary controller.

### *Step 3—Determination of $\beta$ and $\tau$*

When implementing the digital complementary controller, stabilizing condition [8]

$$\tau > (\beta - 1)\frac{T_h}{2} \tag{11}$$

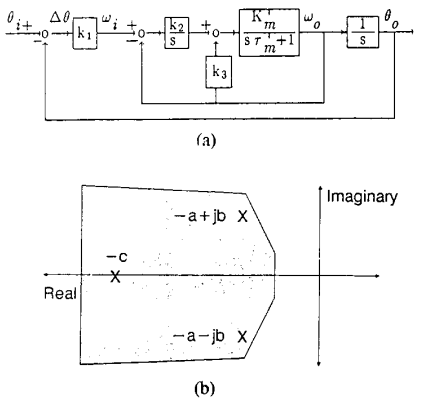


Fig. 8. (a) Simplified system model when plant was compensated by complementary controller. (b) Location of dominant poles.

must be satisfied. For larger $\beta$, $\tau$ must be increased to ensure its stability, but this will deteriorate the performance of the complementary controller. In the designed system the sensitivity reduction gain $\beta$ is set at 10 and the reference model realization time constant $\tau$ is chosen as 10 ms. The open-loop frequency and time responses of the complemented plant under parameter variations are shown in Fig. 7(c) and (d), it can be seen from this figure that significant sensitivity reduction has been obtained by using the complementary controller.

### *Step 4—Determination of $K_1$, $K_2$, and $K_3$*

With the complementary controller, the block diagram of the control system (Fig. 6) can be simplified to Fig. 8(a). According to the design specifications, dominant complex poles $(-a \pm bj)$ with a far away real pole $(-c)$ can be specified as shown in Fig. 8(b) [12]. By using the coefficients comparison method, $K_1$, $K_2$, and $K_3$ can be obtained as functions of $a$, $b$, and $c$.

In the designed system, $-21 \pm j17$ have been chosen as the dominant poles and the far away pole is set at $-300$, $K_1 = 17$, $K_2 = 280$, and $K_3 = 7$ can be easily obtained by coefficients comparison. The closed-loop frequency and unit-step time response of the designed system under parameter variations of Table II is shown in Fig. 9(a) and (b). The pole distribution is shown in Fig. 9(c), and the corresponding numerical values are listed in Table III. It can be observed from Fig. 10 and Table III that the dominant poles are clustered at $-21 \pm j17$ and are insensitive to large parameter and load variations.

## V. Configuration of Experimental System

The configuration of the proposed multimicroprocessor-based ac induction servo drive is shown in Fig. 10. The motor drive system is composed of a power supply, power transistor-based current-controlled inverter (CCI), induction motor, and the multimicroprocessor-based positioning controller.

This multimicroprocessor-based controller is composed of various module control units (MCU's). Each MCU is an 8088-based programmable digital controller. Its detailed circuit schematics is shown in Fig. 11. The MCU communicates with the system controller or other MCU's via the dual-port common memory and a system communication controller. The

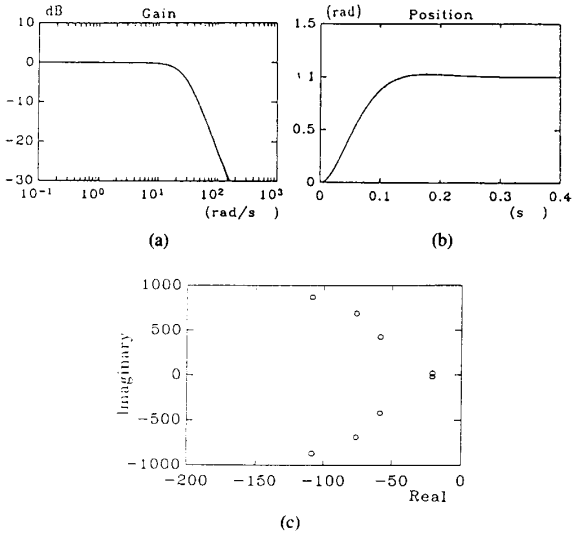


Fig. 9. Closed-loop control system (Fig. 6) under load and parameter variations (Table II). (a) Frequency response. (b) Time response. (c) Pole distribution.

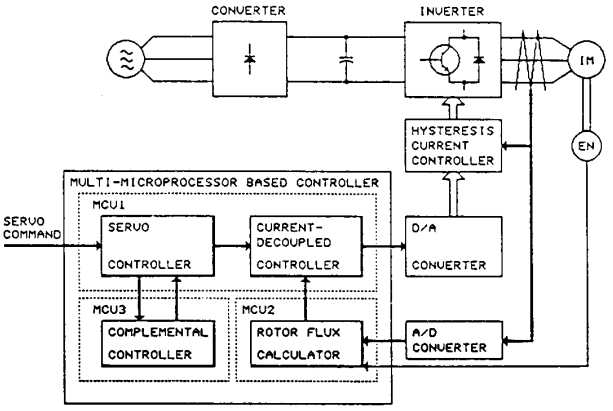


Fig. 10. Configuration of multimicroprocessor-based robust ac induction servo drive.

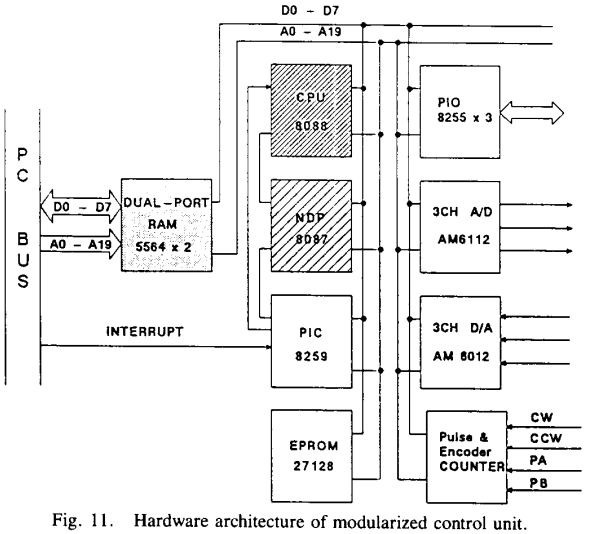


Fig. 11. Hardware architecture of modularized control unit.

TABLE III
CLOSED-LOOP POLES DISTRIBUTION

| | | | |
|---|---|---|---|
| N0 | $P_{1,2} = -20.829 \pm j17.631$ | $P_{3,4} = -174.251 \pm j1607.521$ | $P_5 = -860.466$ |
| N1 | $P_{1,2} = -20.841 \pm j17.638$ | $P_{3,4} = -171.382 \pm j1430.193$ | $P_5 = -866.555$ |
| N2 | $P_{1,2} = -21.099 \pm j17.731$ | $P_{3,4} = -58.619 \pm j423.415$ | $P_5 = -965.764$ |
| N3 | $P_{1,2} = -20.887 \pm j17.655$ | $P_{3,4} = -108.344 \pm j869.509$ | $P_5 = -908.538$ |
| N4 | $P_{1,2} = -20.803 \pm j17.618$ | $P_{3,4} = -181.151 \pm j2299.966$ | $P_5 = -847.093$ |
| N5 | $P_{1,2} = -20.904 \pm j17.655$ | $P_{3,4} = -76.004 \pm j689.033$ | $P_5 = -931.385$ |

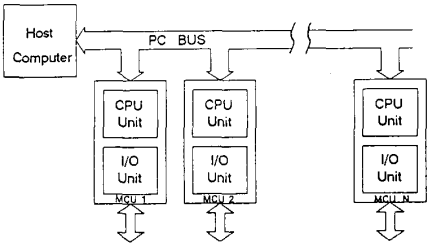


Fig. 12. Dual-port RAM-based multimicroprocessor architecture.

MCU consists of two major parts, one is the CPU unit (CPU-board) which includes the 8088 microprocessor, 8087 numerical data processor, 16K dual-port RAM, 16K EPROM, 8254 programmable interval timer (PIT), and 8259 programmable interrupt controller (PIC). The other is named I/O unit (IO board) which may include programmable digital I/O controller, programmable duty-cycle controller, quadrature photoencoder decoder, A/D, D/A, etc., depends on various applications. The MCU can either be integrated together or work alone, depending on the application.

In the experimental system, a dual-port memory architecture (Fig. 12) has been adopted for the interprocessor communication of this multimicroprocessor system. With this dual-port RAM-based multimicroprocessor system, independent programs can run concurrently and asynchronously. This is beneficial for software development and system integration.

Three MCU's are used for the induction motor position and speed control, as shown in Fig. 10. MCU1, the servo-loop controller, performs two major tasks: 1) servo-loop regulation by software processing of the digital compensator to generate the desired field and torque currents, and 2) torque decoupling control by using the coordinate transformations based on the field-oriented vector control scheme to generate the desired three-phase currents. The power transistor-based CCI regulates the phase currents by using hysteresis control techniques. MCU2, the rotor flux calculator, computes the rotating rotor flux vector based on the flux model as shown in Fig. 2. MCU3, the complementary controller, compensates the parameter and load variations based on the passive adaptive theory [8].

This RAM-based multimicroprocessor controller has advantages of flexibility and modularity. The proposed control structure can be easily implemented on this hardware architecture. Various PWM control strategies, vector control algorithms, and control methods can be independently programmed by software and incorporated into this system. A system controller, which resides on a 16-bit microcomputer, provides task coordination, external interfaces, motion profile control, parameter tuning, and signal recording, and can also be used to monitor the operational status of individual processors.

## VI. Experimental Results

Experimental results of the velocity step response are shown in Fig. 13. The parameters of the induction servo motor used in this experiment are listed in Table IV. Fig. 13 is the dynamic start-stop responses of (a) rotor velocity $\omega_r$, (b) torque current $i_{qs}$, and (c) stator phase current $i_{as}$ of the induction motor from standstill to 1000 r/min. Fig. 13(d)–(f) show the corresponding responses with the motor running from $-1000$ to $+1000$ r/min. The stator phase current is limited to 12 A for protection of the inverter transistors. The dynamic responses of the rotor velocity and torque current show the effectiveness of the software-based decoupling control scheme. Fig. 14 shows the dynamic responses of the induction drive position control under various operating conditions.

Fig. 15 is the steady-state responses when the motor is running at 100 r/min. The magnetic exciting current is set at 3 A when running within the constant-torque operating range. The sinusoidal stator phase current $i_{as}$ and the constant $i_{ds}$ and $i_{qs}$ in the synchronously rotating reference frame show the perfect decouping control of the magnetic and torque current components, and this is the fundamental requirement of high-performance induction servo drive.

Experimental results of the induction motor positioning control under external torque disturbances are shown in Fig. 16. Fig. 16(a) and (b) are the position and corresponding velocity responses of the induction servo motor upon receiving a steplike 4-N·m external torque disturbance by a direct-coupled dc servo motor. This dc servo motor is driven by a current-controlled PWM amplifier. The corresponding torque currents of the dc servo motor and the induction servo motor are shown in Fig. 16(c) and (d), respectively. The robustness of this induction motor position drive can be seen from the fast dynamic responses to external torque disturbances.

## VII. Conclusion

The proposed multiloop complementary control scheme has advantages of robustness and modularity. On the one hand, it combines characteristics of the conventional cascaded servo-loop design techniques with modern robust servo controller design methodology. On the other hand, because of its modularity the proposed method is suitable for multimicroprocessor implementation. An experimental prototype has been implemented to verify the proposed control scheme. Laboratory testing with consideration of large motor parameter and load variations have been carried out. Experimental results have shown the effectiveness of the proposed control scheme and

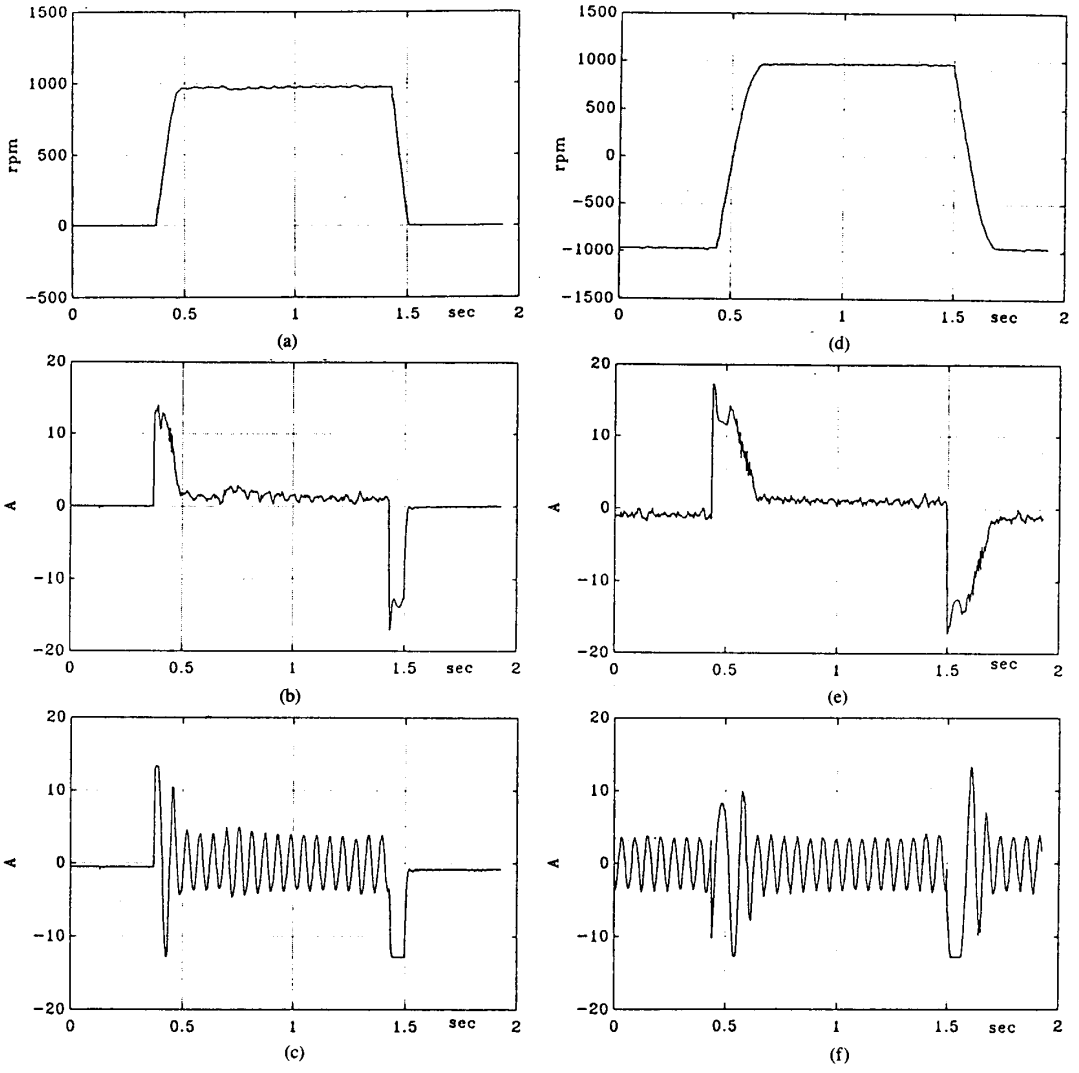


Fig. 13. Dynamic velocity step responses under various operating conditions. (a) Rotor velocity $\omega_r$. (b) Torque current $i_{qs}$. (c) Stator current of phase-$a$ $i_{as}$ of induction motor from standstill to 1000 r/min. (d)–(f) Corresponding responses with motor running from −1000 to +1000 r/min.

TABLE IV
PARAMETERS OF THE INDUCTION SERVO MOTOR

| Type: 3-phase, 2-pole, 800 W Induction Servo Motor | |
|---|---|
| $L_s = 144.6$ mH | $R_s = 1.0\ \Omega$ |
| $L_r = 144.6$ mH | $R_r = 1.3\ \Omega$ |
| $L_m = 136.0$ mH | |

the feasibility of implementing complex control algorithm by using the multimicroprocessor strategy.

## NOMENCLATURE

| | |
|---|---|
| $P$ | Number of poles. |
| $R_s, R_r$ | Stator and rotor resistance. |
| $L_s, L_r$ | Stator and rotor resistance. |
| $L_m$ | Mutual magnetizing inductance. |
| $\sigma_r$ | $=(L_r - L_m)/L_m$, rotor leakage coefficient. |
| $i_{ds}, i_{qs}$ | Stator current in synchronous frame. |
| $\hat{i}_s, \hat{i}_r$ | Stator and rotor current vector. |
| $i_{mr}$ | Magnetizing current. |
| $\hat{\psi}$ | Rotor flux linkage vector. |
| $i_q, i_d$ | Torque and magnetizing current. |
| $\tau_s$ | $=L_s/R_s$, stator time constant. |
| $\tau_r$ | $=L_r/R_r$, rotor time constant. |
| $\tau_e$ | Time constant of current-controlled inverter. |
| $\tau_m$ | Motor load equivalent mechanical time constant. |
| $\tau'_m$ | Time constant of the reference model. |
| $\tau$ | Reference model realization time constant. |
| $K_e$ | Current-controlled inverter gain. |
| $K_m$ | Motor load equivalent gain. |

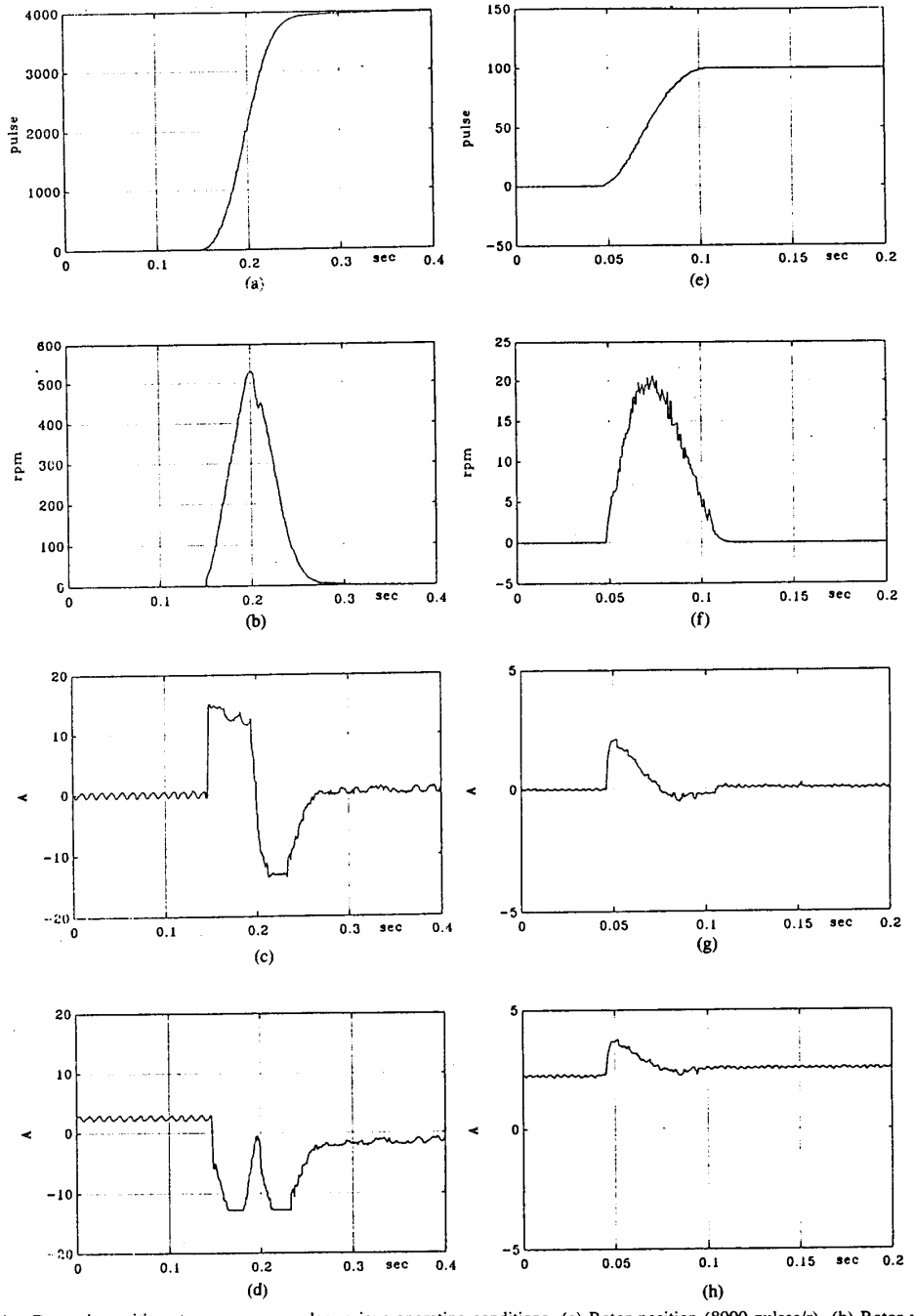


Fig. 14. Dynmaic position step responses under various operating conditions. (a) Rotor position (8000 pulses/r). (b) Rotor velocity $\omega_r$. (c) Torque current $i_{qs}$. (d) Stator current of phase-$a$ $i_{as}$ of induction motor under step positioning command of 4000 pulses. (e)-(h) Corresponding responses for step positioning command of 100 pulses.

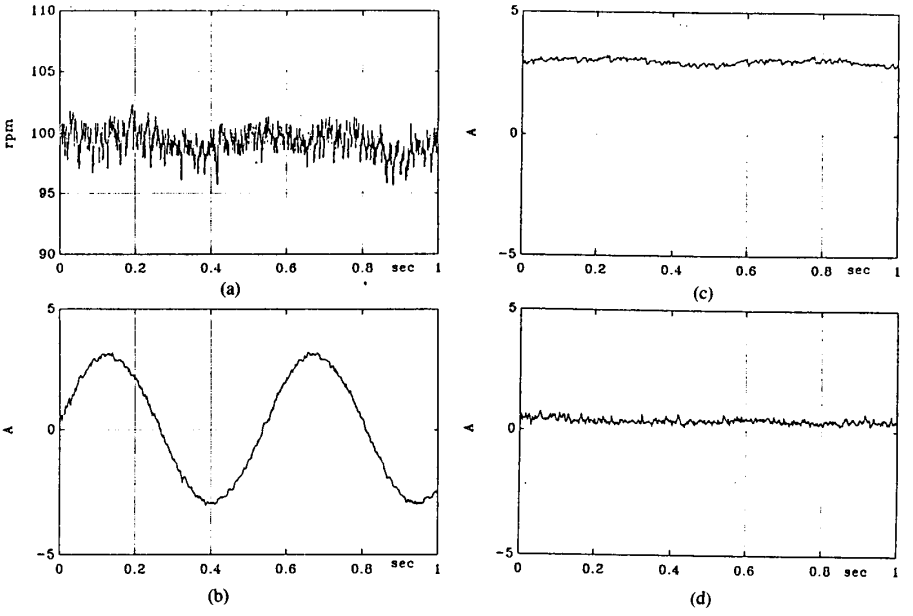


Fig. 15. Steady-state responses with motor running at 100 r/min. (a) Rotor velocity $\omega_r$. (b) Stator current of phase-$a$ $i_{as}$. (c) Field current $i_{ds}$. (d) Torque current $i_{qs}$.

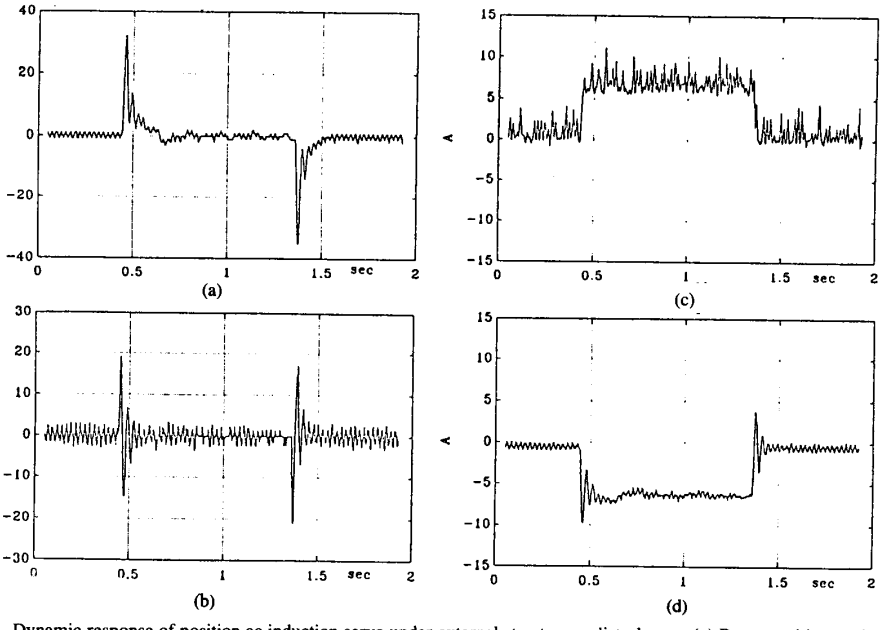


Fig. 16. Dynamic response of position ac induction servo under external step torque disturbance. (a) Rotor position (pulse). (b) Rotor velocity $\omega_r$. (c) DC servo motor armature current $i_a$ ($K_T = 0.539$ N·m/A). (d) Indusction motor torque current component $i_{qs}$.

$K'_m$ Gain of the reference model.
$K_T$ Equivalent torque constant.
$T_e$ Motor developed electrical torque.
$T_l$ Load disturbance torque.
$\omega_e$ Synchronous angular velocity (rad/s).
$\omega_r$ Rotor electrical angular velocity ($(P/2)\omega_m$).
$\omega_m$ Rotor mechanical angular velocity (rad/s).
$\theta_m$ Rotor mechanical angular position (rad).
$T_h$ Sampling period of the digital controller.
$\beta$ Sensitivity reduction gain.

## References

[1] F. Harashima, S. Kondo, K. Ohnishi, M. Kajita, and M. Susono, "Multimicroprocessor-based control system for quick response induction motor drive," *IEEE Trans. Ind. Appl.*, vol. IA-21, no. 3, pp. 602-609, May/June 1985.
[2] K. Kubo, M. Watanabe, T. Ohmae, and K. Kamiyama, "A fully dig-

italized speed regulator using multimicroprocessor system for induction motor drives," *IEEE Trans. Ind. Appl.*, vol. IA-21, no. 4, pp. 1001–1008, July/Aug. 1985.

[3] E. J. Davison and A. Goldenberg, "Robust control of a general servomechanism problem: The servo compensator," *Automatica*, vol. 11, pp. 461–471, 1975.

[4] K. Tamaki, K. Ohishi, K. Ohnishi, and K. Miyachi, "Microprocessor-based robust control of a dc servo motor," *IEEE Contr. Syst. Mag.*, vol. 5, pp. 30–35, Oct. 1986.

[5] H. Naitoh and S. Tadakuma, "Microprocessor-based adjustable-speed DC motor drives using model reference adaptive control," *IEEE Trans. Ind. Appl.*, vol. IA-23, no. 2, pp. 313–318, Mar./Apr. 1987.

[6] I. M. Horowitz, *Synthesis of Feedback Systems*. New York: Academic, 1963, pp. 246–362.

[7] B. A. Francis and W. M. Wonham, "The internal model principle of control theory," *Automatica*, vol. 12, pp. 457–465, 1976.

[8] K. Ohishi, M. Nakao, K. Ohnishi, and K. Miyachi, "Microprocessor controlled dc motor for load insensitive position servo system," *IEEE Trans. Ind. Electron.*, vol. IE-34, no. 1, pp. 44–49, 1987.

[9] S. Bai and R. Tagawa, "Load insensitive electrical position servo: A new design method and its experimental evaluation," in *Proc. IEEE IECON'84*, 1984, pp. 600–605.

[10] F. Blaschke, "The principle of field orientation as applied to the new transvector closed-loop control system for rotating field machines," *Siemens Rev.*, vol. 39, no. 5, pp. 217–220, May 1972.

[11] W. Leonhard, *Control of Electrical Drives*. New York: Springer-Verlag, 1985.

[12] I. B. Huang and K. S. Lu, "Control system synthesis and analysis by approximation to third-order systems," *Int. J. Contr.*, vol. 13, no. 5, pp. 949–959, 1971.

**Ying-Yu Tzou** (S'81–M'88) was born in Taiwan, Republic of China, on February 13, 1956. He received the B.S. and M.S. degrees in control engineering from the National Chiao-Tung University, and the Ph.D. degree in electrical engineering from the Institute of Electronics Engineering of National Chiao-Tung University in 1978, 1983, and 1987, respectively.

During 1980–1981 he was with the Electronic Research and Service Organization of Industry Technology Research Institute as a Design Engineer for the Factory Automation Division. During 1983–1986 he was with Microtek Automation, Inc., as a Project Manager for the development a Computer Numerical Controller for machine tools. He has been an Associate Professor in the Institute of Control Engineering of National Chiao-Tung University since August of 1987. His special area of interest is microprocessor-based motion control system, dc and ac servo drives, power electronics, parallel processing and control, and intelligent and expert control system.

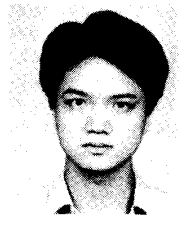

**Hsiang-Jui Wu** was born in Taiwan, Republic of China, on October 7, 1964. He received the B.S. and M.S. degrees in control engineering from the National Chiao-Tung University, Taiwan, in 1986 and 1988, respectively.

Currently, he is working toward the Ph.D. degree at the same university. Among his research interests are field-oriented control, design and control of ac servo drive, digital control theory, and microprocessor applications in control.